



**HAL**  
open science

## Performance analysis of polychromatic laser guide stars used for wavefront tilt sensing

M. Schock, R. Foy, M. Tallon, L. Noethe, J. P. Pique

► **To cite this version:**

M. Schock, R. Foy, M. Tallon, L. Noethe, J. P. Pique. Performance analysis of polychromatic laser guide stars used for wavefront tilt sensing. *Monthly Notices of the Royal Astronomical Society*, 2002, 337 (3), pp.910 - 920. 10.1046/j.1365-8711.2002.05967.x . hal-01118349

**HAL Id: hal-01118349**

**<https://hal.science/hal-01118349>**

Submitted on 11 Dec 2020

**HAL** is a multi-disciplinary open access archive for the deposit and dissemination of scientific research documents, whether they are published or not. The documents may come from teaching and research institutions in France or abroad, or from public or private research centers.

L'archive ouverte pluridisciplinaire **HAL**, est destinée au dépôt et à la diffusion de documents scientifiques de niveau recherche, publiés ou non, émanant des établissements d'enseignement et de recherche français ou étrangers, des laboratoires publics ou privés.

# Performance analysis of polychromatic laser guide stars used for wavefront tilt sensing

M. Schöck,<sup>1\*</sup> R. Foy,<sup>2</sup> M. Tallon,<sup>2</sup> L. Noethe<sup>3</sup> and J.-P. Pique<sup>4</sup>

<sup>1</sup>University of California Irvine, Irvine, CA 92697-4575, USA

<sup>2</sup>CRAL/Observatoire de Lyon, 69561 Saint-Genis-Laval, France

<sup>3</sup>European Southern Observatory, 85748 Garching, Germany

<sup>4</sup>Laboratoire de Spectrométrie Physique (CNRS UMR 5588), Université Joseph Fourier de Grenoble, 38402 Saint Martin d'Hères, France

Accepted 2002 August 11. Received 2002 August 8; in original form 2001 February 1

## ABSTRACT

We present a formalism for performance analyses of adaptive optics systems that use a polychromatic laser guide star to measure the tilt of atmospherically distorted wavefronts. This formalism can be applied to feasibility and design studies of polychromatic laser guide star tip-tilt systems that are used to make the adaptive optics system of a telescope independent of natural guide stars. Using a few simplifying assumptions, the results are presented in analytical form such that a range of system parameters can be studied easily. Directions for the use of more detailed models necessitating numerical calculations are also presented in case more in-depth studies of certain system aspects are desired. Along with the theoretical development, we also present examples of possible solutions of the planned ELP-OA system as well as of an implementation of polychromatic laser guide star systems at large astronomical telescopes.

**Key words:** atmospheric effects – instrumentation: adaptive optics – instrumentation: high angular resolution.

## 1 INTRODUCTION

Over the last decade, many of the large astronomical telescope facilities have begun to implement natural guide star (NGS) adaptive optics (AO) systems and several such systems are now working routinely (see, for example, Bonaccini et al. 1997; Rigaut et al. 1998; Glindemann et al. 2000; Troy et al. 2000; Wizinowich et al. 2000). In theory, the use of AO at large, ground-based telescopes permits diffraction-limited imaging at near-infrared and visible wavelengths. The down side of NGS AO, however, is the generally low sky coverage owing to the need for a bright reference star (Le Louarn et al. 1998).

The solution most commonly proposed for the sky-coverage problem is the use of a laser guide star (LGS) as a reference source (Foy & Labeyrie 1985). While a lot of progress has been made in LGS AO over the last few years, the implementation of LGSs at astronomical sites is still in its initial stages, with only two astronomical sites, Calar Alto (Davies et al. 2000) and Lick (Olivier et al. 1999), ever having had a permanently working system (the Calar Alto LGS has recently been decommissioned). The installation of LGS facilities at some of the large telescopes is progressing (for example at the Keck observatory, where the LGS AO system was recently tested on the sky for the first time) but are still far from being ready for routine use. Besides being complicated from a technical point of view, there are several fundamental problems with LGSs. Here, we only mention the two most severe of these problems: the indeter-

mination problem of the tilt (hereafter simply referred to as the ‘tilt problem’) and the cone effect.

The tilt problem is caused by the inverse return property of light, which makes it impossible to measure the overall wavefront tilt with a single on-axis monochromatic LGS (Pilkington 1987; Séchaud et al. 1988). A number of different solutions to the tilt problem have been proposed and some of them have been pursued experimentally (Esposito et al. 2000; Foy et al. 2000b; Belenkii et al. 1999; Belenkii 2000). In this paper, we examine in detail the use of a polychromatic laser guide star (PLGS) as a possibility to solve the tilt problem (Foy et al. 1995). A PLGS system consists of a laser emission system that excites the mesospheric sodium in such a way that light at different wavelengths is returned. The wavefront tilt is determined from the measurable difference of the tilts at two of the returned wavelengths.

The second fundamental restriction of LGS AO, the cone effect, is produced by the finite height of the LGS, causing the light from the LGS to traverse a different portion of turbulence than the light coming from an astronomical object. The result is an imperfect wavefront correction (Foy & Labeyrie 1985; Tallon & Foy 1990; Tallon, Foy & Vernin 1992; Ellerbroek 1994). The solution proposed for the cone effect is multiconjugate adaptive optics (MCAO) in combination with turbulence tomography (Beckers 1988; Tallon & Foy 1990). The project presented in this paper is a study of the applicability of the PLGS concept to large telescopes for which MCAO is generally considered indispensable. When we are talking about PLGS systems at large telescopes, we therefore assume that the PLGS will be part of an MCAO system. There will then be no significant cone effect.

\*E-mail: mschoeck@uci.edu

The work presented here is done within the framework of the ELP-OA (Étoile Laser Polychromatique et Optique Adaptative) project. The overall goal of ELP-OA is the experimental verification that the measurement of the wavefront tilt using a PLGS without any NGSs is possible at an astronomical telescope facility. ELP-OA consists of two phases, a feasibility phase (Phase 1) and an implementation phase (Phase 2). Phase 1 was officially concluded in December of 1999 and included theoretical treatments of the problem (general theoretical models as well as sodium excitation codes) and several feasibility experiments: two photon return flux experiments from PLGSs in the mesosphere (PASS-1 and PASS-2), an experiment measuring the polychromatic tilt difference along horizontal paths with a laser (MaTiD), a telescope vibration experiment using a pendular seismometer, a number of laser experiments and a laboratory sodium excitation experiment. Detailed descriptions of ELP-OA and its feasibility experiments are given in Foy et al. (2000a), Schöck et al. (1999), Vaillant, Thiébaud & Tallon (2000), and Tokovinin (2000). Sodium excitation codes are described by Bellanger (2002).

In Phase 2 of ELP-OA, we plan to build a prototype astronomical AO system that measures the wavefront tilt without using an NGS. This second phase has two main objectives. First, we want to show that tilt measurements with a PLGS are generally possible. Secondly, ELP-OA should provide sufficient results to serve as a feasibility study for the implementation of a PLGS system at large astronomical telescopes. A third goal, the production of tilt-corrected long-exposure astronomical images without the use of an NGS, is subject to funding at this time.

In this paper we present a formalism that can be used to predict the performance of a PLGS AO system. This formalism was developed as part of the design studies of the ELP-OA system. In Section 2, we set up the emission system and derive the intensity of the laser light in the mesosphere. We describe how we use the results from the feasibility phase of ELP-OA to deduct the return flux at the reception telescope in Section 3. This flux, assumed to be coming from the diffraction-limited core of the laser spot in the mesosphere, is used in Section 4 to derive the optimal integration time and Strehl ratio of the tilt correction system. In subsections of Sections 2–4 we apply the theory to possible Phase-2 ELP-OA setups. The formalism is then also applied to examples of the implementation of a PLGS tilt sensing system at large telescopes at good astronomical sites (Section 5). The paper is concluded in Section 6.

## 2 THE EMISSION SYSTEM

We restrict ourselves to the case of the two-colour excitation of mesospheric sodium with lasers of 569 and 589 nm wavelength, thus exciting the sodium atoms into the  $4D_{5/2}$  state. This excitation was determined by Foy et al. (1995) to be the most promising scenario for tilt correction with a PLGS. The radiative cascade resulting from the return of the atom into its ground state produces photons with wavelengths between 330 and 2338 nm. In spite of our restriction to this particular case, the equations presented in this paper can nevertheless also be used for different two-colour excitation processes (Foy et al. 1995; Biegert, Diels & Milonni 2000; Froc et al. 2000).

The laser wavelengths used here, 569 and 589 nm, are sufficiently close to each other that we can work with the average wavelength  $\lambda_e = 579$  nm. The error introduced by this approximation is negligible with respect to the uncertainties in other parts of the calculations.

Throughout both phases of ELP-OA we work with pulsed lasers with pulse lengths,  $\tau_p$ , of the order of tens of nanoseconds and

pulse repetition rates,  $f_{\text{rep}}$ , of the order of tens of kilohertz. We assume that each laser produces light of average power  $P$  at the laser output. The instantaneous laser power in the mesosphere is then  $r_{579}\eta_{579}P/\delta$  per laser colour, where  $r_{579}$  is the reflectivity of the emission optics system at 579 nm and  $\eta_{579}$  is the atmospheric transmission coefficient at 579 nm.  $\delta = \tau_p f_{\text{rep}}$  is the duty cycle of the laser.

We assume that a telescope of diameter  $D_e$  is used to project the two laser beams into the mesosphere. No assumption is made a priori as to whether this telescope is the same as the telescope used for the tilt measurements and astronomical observations. The only assumption made concerning the relation of the emission and reception telescopes is that they are separated by a sufficiently small distance that projection effects can be ignored.

We will see in Section 4 that it is advantageous to produce the smallest possible laser spot in the mesosphere. For the cases considered in this paper, we assume emission telescopes of 25–50 cm diameter. These diameters are generally a few times larger than Fried’s parameter,  $r_0$ , at the sites of interest. In the examples treated in this paper we therefore assume that we use of a low-order AO system for emission in order to reduce the mesospheric spot size. In the following, we nevertheless also introduce the equations necessary for the case of emitting without an AO system.

We assume that the spot in the mesosphere consists of a diffraction-limited core and a seeing-limited halo. A fraction  $S_e r_{579}\eta_{579}P/\delta$  of the laser power, where  $S_e$  is the Strehl ratio achieved by the emission system, is in the core, whereas the rest,  $(1 - S_e)r_{579}\eta_{579}P/\delta$ , is in the halo. Using the equivalent widths of the spot as the diameters of the core and the halo,  $d_c$  and  $d_h$ , in the mesosphere we can write

$$d_{c/h} = \frac{4}{\pi} \frac{\lambda_e}{x \cos(\theta)} h, \quad (1)$$

where  $h \approx 90$  km is the altitude of the mesospheric sodium layer and  $\theta$  is the zenith angle.  $x$  equals the aperture diameter of the emission telescope,  $D_e$ , in the case of the diffraction-limited core, whereas it equals  $r_0$  for the seeing-limited halo.

The intensity in the mesosphere can thus be approximated as consisting of two parts, a coherent core with average intensity

$$I_c = \frac{\pi r_{579}\eta_{579} \cos^2(\theta) D_e^2 S_e P}{4 \lambda_e^2 h^2 \delta} \quad (2)$$

and a halo of intensity

$$I_h = \frac{\pi r_{579}\eta_{579} \cos^2(\theta) r_0^2 (1 - S_e) P}{4 \lambda_e^2 h^2 \delta}. \quad (3)$$

In reality, the intensities in the core and halo of the laser spot are, of course, not spatially constant, but are different at every point in the mesosphere. In the case of perfect wavefront correction by the emission system, the intensity distribution is an Airy disc. In the case of no or partial AO correction, the intensity distribution is irregular and, additionally, not constant in time. We will come back to this point in Section 3.

We also point out that the above application of the Strehl ratio to the calculation of the intensities is not strictly correct and the coherent energy,  $CE$ , should be used instead. However, because we are dealing with cases of large Strehl ratios,  $CE \approx S_e$  is a valid approximation.

### 2.1 Laser intensity expected for ELP-OA

Phase 2 of ELP-OA will take place at the Observatoire de Haute Provence (OHP) in southern France using the 1.52-m telescope and

**Table 1.** Parameters of the systems investigated in this paper. All atmospheric parameters are given for a wavelength of 0.5  $\mu\text{m}$ .

|  | ELP-OA I                | ELP-OA II                 | ELP-OA III                | 8-m I                     | 8-m II                    |
|--|-------------------------|---------------------------|---------------------------|---------------------------|---------------------------|
| $P$ (W)                                    | 25                      | 25                        | 25                        | 25                        | 25                        |
| Polarization                               | Linear                  | Left circular             | Modeless                  | Left circular             | Modeless                  |
| $f_{\text{rep}}$ (kHz)                     | 15                      | 30                        | 30                        | 30                        | 30                        |
| $\tau_p$ (ns)                              | 50                      | 80                        | 80                        | 80                        | 80                        |
| $\lambda_e$ (nm)                           | 579                     | 579                       | 579                       | 579                       | 579                       |
| $D_e$ (m)                                  | 0.25                    | 0.25                      | 0.25                      | 0.5                       | 0.5                       |
| $r_0$ (cm)                                 | 5–11                    | 5–11                      | 5–11                      | 15–25                     | 15–25                     |
| $D_e/r_0$                                  | 2–5                     | 2–5                       | 2–5                       | 2–3                       | 2–3                       |
| $f_{\text{TZ}}$ (Hz)                       | 4.5–9.5                 | 4.5–9.5                   | 4.5–9.5                   | 1.9–2.9                   | 1.9–2.9                   |
| $r_{579}$                                  | 0.9                     | 0.9                       | 0.9                       | 0.9                       | 0.9                       |
| $\eta_{579}$                               | 0.8                     | 0.8                       | 0.8                       | 1                         | 1                         |
| $\theta$                                   | 0                       | 0                         | 0                         | 0                         | 0                         |
| $\Phi_P$ ( $\text{s}^{-1} \text{m}^{-2}$ ) | $\approx 5 \times 10^4$ | $\approx 2.2 \times 10^5$ | $\approx 2.2 \times 10^6$ | $\approx 7.0 \times 10^4$ | $\approx 7.0 \times 10^5$ |
| $D_r$ (m)                                  | 1.52                    | 1.52                      | 1.52                      | 8.0                       | 8.0                       |
| $(n-1)/\Delta n$                           | 25                      | 18                        | 18                        | 18                        | 18                        |
| $\eta$                                     | 0.08                    | 0.08                      | 0.08                      | 0.13                      | 0.13                      |
| $t_{i,\text{max}}$ (ms)                    | 92                      | 35                        | 12–19                     | 42–56                     | 20–26                     |

an adaptive optics system that was developed at the Observatoire de la Côte d’Azur (Verinaud, Blazit & Mourard 2000). The original, non-optimized ELP-OA system, as planned before the start of Phase 1, provides for the use of CuHBr lasers (Coutance, Naylor & Pique 1995; Coutance & Pique 1998) with powers  $P = 25$  W per emission wavelength, pulse repetition rate  $f_{\text{rep}} \approx 15$  kHz and pulse length  $\tau_p = 50$  ns. We assume here that the laser beams are emitted through a 0.25-m aperture with a low-order AO system, although it is not yet clear whether ELP-OA will indeed be realized in this way. All parameters of this system, hereafter referred to as ‘ELP-OA I’, as well as of the other systems investigated in this paper are summarized in Table 1.

The OHP is located at the relatively low altitude of 650 m and has decent seeing conditions for a low-altitude site. It is nevertheless not comparable to high-altitude sites. Values of  $r_0$  range from approximately 5 cm under bad seeing conditions to 11 cm in very good seeing conditions, thus resulting in  $D_e/r_0$  values of between 2 and 5. For such values of  $D_e/r_0$ , even an emission AO system correcting only for the three second-order Zernike terms can produce long-exposure Strehl ratios of between 0.2 (in bad seeing conditions) and close to unity (in good seeing conditions; Roddier (1993)). We will see in Sections 4.1 and 5 that exposure times of the reception system are of the order of tens of milliseconds. We are therefore dealing with cases intermediate between long and short exposures and the Strehl ratio of the ELP-OA emission system will be significantly closer to unity than the long-exposure values given by Roddier. Thus, even correcting only the defocus and third-order astigmatism terms, we arrive at a basically diffraction-limited laser spot under good and medium seeing conditions. If we correct seven Zernike terms (the first nine terms minus tip and tilt), we obtain a diffraction-limited laser spot under most if not all seeing conditions. In all examples in this paper we will therefore assume that the emission system produces a diffraction-limited laser spot in the mesosphere and that  $S_e = 1$  in equation (2).

Because only a small-wavelength range needs to be covered by the emission optics (569–589 nm), special coatings can be used that have a very high reflectivity. Even with the possibly large number of reflections necessary for an emission AO system, we will therefore have a high overall reflectivity of the emission system. Here, we

assume  $r_{579} = 0.9$ . The atmospheric transmission at 579 nm at a low-altitude site is  $\eta_{579} \approx 0.8$  (Allen 1976). We restrict ourselves to the case of emission towards the zenith. We thus arrive at an intensity in the mesosphere of  $I_c = 4.3 \times 10^5 \text{ W m}^{-2}$  in a spot of approximately 25 cm diameter.

We compare this intensity to the intensity of the PASS-1 experiment, where we had  $P_{\text{max}} = 175$  W,  $f_{\text{rep}} = 4.3$  or 12.9 kHz,  $\tau_p = 50$  ns,  $r_{579} \approx 0.8$  and  $\eta_{579} \approx 0.9$ . The size of the emission beam was approximately  $4 \times 8 \text{ cm}^2$  and  $r_0$  was measured to be of the order of 6 cm (Foy et al. 2000b). Using  $D_e \approx r_0 \approx 6$  cm and equation (1) (multiplied by  $\sqrt{2}$  to account for the combined effects of atmospheric and emission optics diffraction), yields a spot diameter of approximately 1.5 m and laser intensities of  $1.0 \times 10^5 \text{ W m}^{-2}$  for  $f_{\text{rep}} = 12.9$  kHz and  $3.1 \times 10^5 \text{ W m}^{-2}$  for  $f_{\text{rep}} = 4.3$  kHz. In the next section, we use the fact that the laser intensities of PASS-1 and ELP-OA are similar to estimate the expected photon return flux from the PLGS for ELP-OA.

### 3 PHOTON RETURN FLUX

Obtaining the PLGS photon return flux,  $\Phi_p$ , from the laser intensity in the mesosphere is not a trivial problem and cannot be put into simple equations. Detailed treatments, both theoretical and experimental, of the return flux from monochromatic sodium LGSs are available in the literature (for example in Morris 1994; Avicola et al. 1994; Fugate et al. 1994; Milonni, Fugate & Telle 1998). However, no such information was available for the PLGS until recently and was one of the major objectives of Phase 1 of ELP-OA. We now have experimental results available from the two PASS experiments (Foy et al. 2000a,b) and from theoretical simulations (Froc et al. 2000; Bellanger 2002). Experimental and theoretical results are consistent with each other and both can theoretically be used to obtain the return flux expected from the PLGS.

In this paper we use the results obtained from our experimental data. In that case, we do not have to take the non-constant spatial intensity distribution in the mesosphere into account if we assume that the shape of the intensity distributions as well as their temporal variations are comparable between the PASS experiments and the setup investigated here. At equal instantaneous laser intensity in the

**Table 2.** Saturation intensities for sodium under mesospheric conditions.  $\lambda_c$  is the laser wavelength,  $I_{\text{sat},m}$  is the saturation intensity of sodium per homogeneous linewidth (mode),  $\Delta\nu_L$  is the total linewidth including hyperfine structure splitting and Doppler broadening of sodium under mesospheric conditions,  $\Delta\nu_H$  is the homogeneous linewidth of the sodium transitions,  $N_M$  is the total number of modes and  $I_{\text{sat}}$  is the overall saturation intensity of mesospheric sodium. See Foy et al. (1995) for details.

| Transition   | 3S–3P <sub>3/2</sub> | 3P <sub>3/2</sub> –4D <sub>5/2</sub> |
|--|----------------------|--------------------------------------|
| $\lambda_c$ (nm)   | 589                  | 569                                  |
| $I_{\text{sat},m}$ (W m <sup>-2</sup> )                      | 185                  | 475                                  |
| $\Delta\nu_L$ (GHz)  | ≈3                   | ≈1                                   |
| $\Delta\nu_H$ (MHz)  | 10                   | 16                                   |
| $N_M = \Delta\nu_L/\Delta\nu_H$                              | 300                  | 83                                   |
| $I_{\text{sat}} = N_M I_{\text{sat},m}$ (W m <sup>-2</sup> ) | $5.6 \times 10^4$    | $3.7 \times 10^4$                    |

mesosphere, the return flux will then simply scale with the laser spot size, the pulse repetition rate and the pulse length (see below). If, on the other hand, theoretical models were used, simulations of the intensities at each point in the mesosphere and the respective return fluxes were necessary. While such a treatment might be desirable in the final design phase of a PLGS AO system, it is well beyond the intention of this paper.

### 3.1 Expected photon return flux for ELP-OA

As we have shown in Section 2.1, the laser intensity in the mesosphere during the PASS-1 experiment for a pulse repetition rate of 4.3 kHz,  $I_c^{\text{PASS-1}}$ , is slightly smaller than the expected intensity for ELP-OA,  $I_c^{\text{ELP-OA}}$ , while both intensities are much larger than the saturation intensity of mesospheric sodium (see Table 2). In the saturated regime, the return flux from the PLGS will vary only slowly with  $I_c$ . We can therefore use the return flux found during PASS-1 at 4.3 kHz,  $\Phi_p^{\text{PASS-1}} = 5 \times 10^5$  photon s<sup>-2</sup> m<sup>-2</sup> (see fig. 5 in Foy et al. 2000b) for ELP-OA with little error. Note that we have used the maximum of the three values found for the relevant PASS-1 configuration because  $I_c^{\text{ELP-OA}}$  is greater than  $I_c^{\text{PASS-1}}$ .

$\Phi_p^{\text{PASS-1}}$  is, however, not equal to the return flux expected for ELP-OA,  $\Phi_p^{\text{ELP-OA}}$ , because there exist differences in the repetition rate, mesospheric spot size and laser frequency modulation between PASS-1 and ELP-OA. Because the instantaneous laser intensities in the mesosphere are approximately equal for PASS-1 and ELP-OA, the dependence on the spot size and repetition rate is a simple scaling given by  $\Phi_p^{\text{ELP-OA}}/\Phi_p^{\text{PASS-1}} = (f_{\text{rep}}^{\text{ELP-OA}}/f_{\text{rep}}^{\text{PASS-1}})(A^{\text{ELP-OA}}/A^{\text{PASS-1}})$ , where  $A$  denotes the respective laser spot areas in the mesosphere.

The dependence of the return flux on frequency modulation is more complicated than that. During PASS-1, in order to excite several velocity classes of the mesospheric sodium, the spectral lines of the single-mode lasers were phase modulated with two sine waves, one at 125 MHz and another at 300 MHz (Friedman 1999, private communication). PASS-2 and laboratory experiments have shown that this return flux cannot be increased by more than a factor of 2 by changing the phase modulation. In fact, the entire Doppler spectrum of mesospheric sodium cannot be continuously covered by a phase modulated nanosecond laser because the frequency of the modulation is limited on one hand by the inverse of the pulse duration (the phase must oscillate at least several times during the pulse) and on the other hand by the Doppler width (larger phase modulation frequencies generate spectral modes outside the resonance transition). The situation in the second phase of ELP-OA will therefore be comparable to PASS-1. We thus arrive at an expected return flux

of approximately  $5 \times 10^4$  photon s<sup>-1</sup> m<sup>-2</sup> for the ELP-OA I configuration.

Even with phase modulation, the saturation of the sodium transitions is still a huge limitation. Physically, saturation means that the sodium vapour becomes more transparent. One possibility with which we have experimented is the use of a ‘modeless laser’ (Ewart 1985). Theoretical and experimental simulations (Pique & Soden 2002) have shown that a return flux increase of up to a factor of 10 might be obtained with a ‘modeless laser’. In brief, the saturation parameter  $S_m = I_{c,m}/I_{\text{sat},m}$  per homogeneous linewidth is of the order of several thousands for a single-mode laser, but it can be smaller than 10 for a modeless laser, which is capable of exciting about 300 velocity classes of the 3-GHz linewidth of the 589-nm transition. We believe that the development of an adequate modeless sodium laser is fundamental for the success of ELP-OA and would also be useful for monochromatic laser guide stars. Such a development is in progress at the Laboratoire de Spectrométrie Physique.

## 4 THE RECEPTION SYSTEM

For the reception system we consider a telescope of diameter  $D_r$ . The tilt correction is performed using the diffraction-limited coherent core of the PLGS in the mesosphere. The correction of modes of the wavefront with orders higher than the tilt is assumed to be done by a separate AO system, using a ‘standard’ monochromatic LGS as a reference source. In a practical application, it will certainly be most efficient to use the D<sub>2</sub> component of the PLGS to provide this reference source. Thus, the assumed system works like a standard LGS AO system with a separate tip-tilt and higher-order system, with the only difference from existing systems being that the tilt is measured with a PLGS instead of an NGS.

The goal of this paper is to estimate the expected performance of the tilt correction system. We thus only account for errors caused by the wavefront tilt or the tilt correction system. If no other errors are present, the tilt Strehl ratio,  $S_{\text{tilt}}$ , of an image depends on the variance of the tilt measurement,  $\sigma_{\text{tilt}}^2$ , as (Sandler et al. 1994)

$$S_{\text{tilt}} = \frac{1}{1 + \frac{1}{2}\pi^2\sigma_{\text{tilt}}^2(D_r/\lambda_c)^2}, \quad (4)$$

where  $\lambda_c$  is the wavelength at which the wavefront is corrected. Equation (4) is obtained by using a Gaussian with the same equivalent width as the theoretical, unperturbed laser spot (Airy disc) in the mesosphere. The tilt and thus  $\sigma_{\text{tilt}}^2$  are understood to be in angular units. We point out that  $\lambda_c$  is generally not identical to any of the two wavelengths used for the tilt determination.

The error of the tilt correction is given by

$$\sigma_{\text{tilt}}^2 = \sigma_{\text{ph}}^2 + \sigma_{\text{bw}}^2 + \sigma_{\text{instr}}^2 + \sigma_{\text{cone}}^2, \quad (5)$$

where the dominant error sources are the tilt measurement error (photon noise),  $\sigma_{\text{ph}}^2$ , and the tilt bandwidth error caused by the finite integration time,  $\sigma_{\text{bw}}^2$ . These two errors are treated in detail later in this section.

$\sigma_{\text{instr}}^2$  in equation (5) describes the sum of all instrumental errors. These errors consist primarily of the readout noise and the dark current of the detector. We will see later that, because of the nature of the PLGS tilt determination process, we are dealing with exposure times of at least tens of milliseconds and that we are working in a high-photon regime. Thus we assume here that, when working with a good detector, we can neglect both readout noise and dark current. (We note that the centre-of-gravity method of the tilt determination used in this section has a higher precision if a larger part of the detector, that is, more pixels are used. The readout noise, however,

also increases with the number of pixels. It is thus clear that, for a specific system, a compromise between these two competing effects has to be found.) We also make the assumption that no instrumental biases exist. Thus, in this paper we neglect  $\sigma_{\text{instr}}^2$  with respect to the dominant error sources.

The fourth term in equation (5),  $\sigma_{\text{cone}}^2$ , is the error caused by the tilt cone effect. For ELP-OA, using a 1.52-m telescope, the cone effect is small and can be neglected. For an 8-m-class telescope, a single laser guide star produces non-acceptable wavefront distortions owing to the cone effect even if the tilt is measured with an NGS. We therefore assume that the PLGS will be implemented at a large telescope only in combination with an MCAO system. There will then be no significant contribution of  $\sigma_{\text{cone}}^2$  to the error budget.

The last error is caused by the seeing-limited halo of the laser spot in the mesosphere. As described in Section 2, we only deal with systems in this paper that produce a very high Strehl ratio for the emission system. We can therefore assume that virtually all photons come from the core of the mesospheric laser spot and that we can neglect the halo. We will nevertheless set up the equations for taking it into account in Appendix A, in case our formalism is to be applied to an emission system with  $D/r_0 \gg 1$  and/or without an emission AO system.

Using the assumptions made above, the total tilt error is now given by  $\sigma_{\text{tilt}}^2 = \sigma_{\text{ph}}^2 + \sigma_{\text{bw}}^2$ . Foy et al. (1995) have shown that

$$\sigma_{\text{ph}}^2 = \sigma_{\text{diff tilt}}^2 \left( \frac{n-1}{\Delta n} \right)^2, \quad (6)$$

where  $\sigma_{\text{diff tilt}}^2$  is the variance of the differential tilt measurement,  $n$  is the refractive index of air and  $\Delta n$  is the difference in  $n$  between the two colours of the PLGS. [ $(n-1)/\Delta n$  takes on values of 18 and 25 for the cases considered in this paper; see Table 1.] The differential tilt is defined as the difference of the tilts at two different wavelengths caused by the chromatic properties of the refractive index of air. If we determine the tilt at each wavelength from the centre of gravity of the PLGS images, we obtain

$$\sigma_{\text{diff tilt}}^2 = \frac{\sigma_{\text{spot}}^2(\lambda_1)}{N(\lambda_1)} + \frac{\sigma_{\text{spot}}^2(\lambda_2)}{N(\lambda_2)}, \quad (7)$$

where  $\sigma_{\text{spot}}(\lambda)$  is the angular radius (defined as the standard deviation of a Gaussian with the same equivalent width as the respective Airy disc) of the laser spot on the detector and  $N(\lambda)$  is the number of photons returned from the PLGS.  $\lambda_1$  and  $\lambda_2$  are the two wavelengths used for the tilt determination.

For the systems considered in this paper, we always have  $D_r \gg D_e$ . Thus, the spot in the mesosphere will always be resolved by the reception telescope.  $\sigma_{\text{spot}}$  is then given by

$$\sigma_{\text{spot}} = \frac{\sqrt{2} \lambda_e}{\pi D_e} \quad (8)$$

and is independent of the wavelength of the returned light.

Ignoring the central obscuration,

$$N(\lambda) = \eta(\lambda) \Phi_P(\lambda) \pi (D_r/2)^2 t_i, \quad (9)$$

where  $\eta(\lambda)$  is the combined transmissivity of the atmosphere and the instrument and  $\Phi_P(\lambda)$  is, as before, the return flux from the PLGS (before taking the atmospheric transmissivity into account), both at wavelength  $\lambda$ .  $t_i$  is the integration time. Owing to the wavelength dependence of the atmospheric transmission and the nature of the two-colour sodium excitation process used here (Foy et al. 1995), the number at photons at 330 nm and at the  $D_1$  line (589.6 nm), which are the two lines most easily observed from a technical point of view, arriving at the reception telescope are essentially equal.

The two terms in equation (7) are therefore approximately equal and we can work with twice the term obtained for  $\lambda_1 = 330$  nm, which is the wavelength that we observed most carefully during the PASS experiments. For simplicity, we will therefore stop writing the explicit wavelength dependences in equations (7) and (9) and assume that  $\eta$  and  $\Phi_P$  are the transmissivity and the return flux at 330 nm. Combining all of this we obtain

$$\sigma_{\text{ph}}^2 = \left( \frac{n-1}{\Delta n} \right)^2 \frac{16}{\pi^3} \frac{\lambda_e^2}{\eta \Phi_P D_e^2 D_r^2 t_i}. \quad (10)$$

The next step is the calculation of the variance of the one-dimensional jitter of the Z-tilt,  $\sigma_{\text{bw}}^2$ . (We need to use the Z-tilt for our calculation as the higher-order Zernike terms are assumed to be corrected by another AO system. Because the two systems have to be independent, the modes corrected by the systems need to be mutually orthogonal.) If  $\Phi_Z$  is the one-dimensional power spectrum and  $E$  is the error transfer function defined in equation (18) below,  $\sigma_{\text{bw}}^2$  is given by

$$\sigma_{\text{bw}}^2 = \int_0^\infty \Phi_Z(f) |E(f)|^2 df. \quad (11)$$

We use the expression given by Tyler (1994) for the power spectrum, but with the simplifying assumption of a constant wind speed,  $V(h)$ , at all altitudes,  $h$ .<sup>1</sup> With the definition  $v = V/D_r$  one finds

$$\Phi_Z(f) = 1.85 \left( \frac{\lambda_c}{D_r} \right)^2 f_{\text{TZ}}^2 v^{5/3} f^{-14/3} F_Z(f/v) \quad (12)$$

with

$$F_Z(f/v) = \int_0^1 dx \frac{x^{11/3}}{\sqrt{1-x^2}} J_2^2 \left( \frac{\pi f}{x v} \right). \quad (13)$$

Using again the simplifying assumption of a constant wind speed at all altitudes, the atmospheric tilt coherence frequency,  $f_{\text{TZ}}$  (analogous to the Greenwood frequency but only considering the tilt component of the distorted wavefront) in equation (12) is given by

$$f_{\text{TZ}} = 0.368 D_r^{-1/6} \lambda_c^{-1} V \sec^{1/2} \theta \left[ \int dh C_n^2(h) \right]^{1/2}, \quad (14)$$

where  $C_n^2(h)$  is the turbulence structure constant as a function of altitude. With the definition

$$r_0 = 0.185 \left[ \lambda_c^{-2} \sec^2(\theta) \int dh C_n^2(h) \right]^{-3/5}, \quad (15)$$

the atmospheric tilt coherence frequency can then be written as

$$f_{\text{TZ}} = 0.0902 \left( \frac{r_0}{D_r} \right)^{1/6} \left( \frac{V}{r_0} \right). \quad (16)$$

The control loop of the system investigated here consists of an integration of the tilt over an integration time  $t_i$  and an immediate correction with a tip/tilt mirror. Immediate correction means that all the delays caused by the readout of the charge-coupled device (CCD), the calculation of the tilt value, and the setting of the mirror are neglected. This is, in view of the relatively large integration times of the order of tens of milliseconds (see Section 4.1), certainly

<sup>1</sup>It is fairly common to use the approximate tilt power spectrum; that is, the power spectrum consisting of the high- and low-frequency limit asymptotes, to perform calculations like this because the integrals become much simpler by doing this. However, this introduces errors of more than 40 per cent into the calculation of  $\sigma_{\text{bw}}^2$ . The use of the exact power spectrum is therefore necessary in this calculation.

a justified assumption. The common open-loop transfer function  $H$  used for this type of control loop (Parenti & Sasiela 1994) is the product of a factor describing the averaging of the signal during the integration time and an integrator describing the summation of the signals on the tip/tilt mirror,

$$H(f) = g \frac{1 - e^{-i2\pi f t_i}}{(i2\pi f t_i)^2}, \quad (17)$$

where  $g$  is a gain factor. With standard techniques it can be shown that, with a gain of  $g = 1$ , the closed control loop is stable. (Note that this transfer function describes exactly a control loop where, in the limit  $n \rightarrow \infty$  and  $t_i \rightarrow 0$ , the signal is the sliding average over integration times  $nt_i$  and the gain is  $1/n$ . We have performed numerical simulations to confirm that this description is also sufficiently accurate for the basic control loop with  $n = 1$  that is outlined above.) The error transfer function used in equation (11) is then given by (Parenti & Sasiela 1994)

$$|E(f)|^2 = \left| \frac{1}{1 + H} \right|^2 = \frac{(2\pi f t_i)^2}{4 \sin^2(\pi f t_i) [1/(2\pi f t_i)^2 - 1] + (2\pi f t_i)^2}. \quad (18)$$

In the limit of small products  $f t_i$ , that is, in the high-bandwidth limit, the error transfer function can be approximated by

$$|E_{\text{high}}(f)|^2 = (2\pi f t_i)^2 = \left( \frac{f}{f_c} \right)^2, \quad (19)$$

where  $f_c = 1/(2\pi t_i)$  is defined as the frequency where this function cuts the 0 dB line. Using  $E_{\text{high}}$ , Tyler (1994) has shown that  $\sigma_{\text{bw,high}}$  is given by

$$\sigma_{\text{bw,high}}^2 = (f_{\text{TZ}}/f_c)^2 (\lambda_c/D_r)^2. \quad (20)$$

We now combine equations (4), (10) and (20) and find the overall tilt Strehl ratio of the system,

$$S_{\text{tilt}} = \left[ 1 + \frac{\pi^2}{2} (\sigma_{\text{ph}}^2 + \sigma_{\text{bw}}^2) \left( \frac{D_r}{\lambda_c} \right)^2 \right]^{-1} = \left[ 1 + \left( \frac{n-1}{\Delta n} \right)^2 \frac{8}{\pi} \frac{\lambda_c^2}{\eta \Phi_P D_e^2 \lambda_c^2 t_i} + 2\pi^4 f_{\text{TZ}}^2 t_i^2 \right]^{-1}. \quad (21)$$

We simplify equation (21) by introducing the constants

$$a = \left( \frac{n-1}{\Delta n} \right)^2 \frac{8}{\pi} \frac{\lambda_c^2}{\eta \Phi_P D_e^2 \lambda_c^2} \quad b = 2\pi^4 f_{\text{TZ}}^2$$

for convenience for the following calculations. We then have

$$S_{\text{tilt}} = \frac{1}{1 + a/t_i + b t_i^2}, \quad (22)$$

in which we notice the expected competing effects of measurement and bandwidth errors. The final step is to determine the integration time,  $t_{i,\text{max}}$ , for which a maximum  $S_{\text{tilt}}$  is obtained. The Strehl ratio is maximum when  $\sigma_{\text{tilt}}^2$  in equation (4) takes on its minimum value and we easily show that

$$t_{i,\text{max}} = \left( \frac{a}{2b} \right)^{1/3} = 0.187 \left[ \left( \frac{n-1}{\Delta n} \right)^2 \frac{\lambda_c^2}{\eta \Phi_P D_e^2 \lambda_c^2 f_{\text{TZ}}^2} \right]^{1/3}. \quad (23)$$

Thus, we arrive at a simple analytical solution for determining the maximum Strehl ratio of the tilt correction system in the high-bandwidth limit.

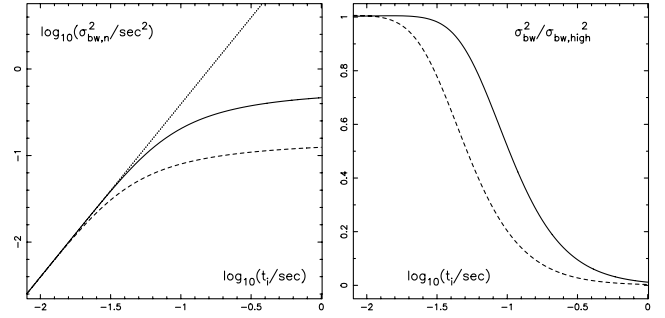


**Figure 1.** Left: normalized bandwidth error as a function of the integration time,  $t_i$ , calculated numerically from the power spectrum in the high-bandwidth limit ( $\sigma_{\text{bw,n,high}}^2$ , dotted line) and using the error transfer function  $E(f)$  for ratios  $V/D_r = 6.12 \text{ s}^{-1}$  ( $\sigma_{\text{bw,n,1}}^2$ , solid line) and  $V/D_r = 12.24 \text{ s}^{-1}$  ( $\sigma_{\text{bw,n,2}}^2$ , dashed line), right: ratios  $\sigma_{\text{bw,n,1}}^2/\sigma_{\text{bw,n,high}}^2$  (solid line) and  $\sigma_{\text{bw,n,2}}^2/\sigma_{\text{bw,n,high}}^2$  (dashed line).

Equations (20)–(23) are, however, not applicable to all cases treated in this paper because the system bandwidth is not significantly higher than the tilt coherence time for all of them. We have therefore also evaluated the integral in equation (11) numerically using the power spectrum given by equation (12) and the error transfer function given by equation (18) with gain  $g = 1$ . The results are shown in Fig. 1. The plot on the left shows the normalized functions

$$\sigma_{\text{bw,n}}^2 = \sigma_{\text{bw}}^2 \left( \frac{D_r}{\lambda_c} \right)^2 \left( \frac{1}{f_{\text{TZ}}} \right)^2. \quad (24)$$

The dotted line is the high-bandwidth limit given by equation (20) which is proportional to  $(2\pi t_i)^2$  and therefore shows up as a straight line in the figure. The two other lines are the results of the numerical integration of  $\sigma_{\text{bw,n}}^2$  with ratios  $V/D_r = 9.3/(1.52 \text{ s}) = 6.12 \text{ s}^{-1}$  (solid line) and  $V/D_r = 12.24 \text{ s}^{-1}$  (dashed line) as functions of the integration time  $t_i$ . The first value of  $V/D_r$  was chosen because it is the value used in most of the examples in Section 4.1. The second value was chosen to show how changing  $V/D_r$  by a factor of 2 affects  $\sigma_{\text{bw,n}}^2$ .

The plots on the right-hand side of Fig. 1 show the ratios of the exact bandwidth error to the bandwidth errors in the high-bandwidth limit. The integration time for which the ratios attain a given value is roughly inversely proportional to the ratio  $V/D_r$ . We can see that the approximation only works well for integration times up to approximately 50 ms for the values of  $D/r_0$  of interest in this paper. If we cannot make the approximations of the high-bandwidth limit, no analytical solution for the maximum Strehl ratio exists. The easiest way of dealing with this case is to modify equation (22) to

$$S_{\text{tilt}} = \frac{1}{1 + a/t_i + c(t_i) b t_i^2}, \quad (25)$$

where  $c(t_i)$  is a correction factor that is equal to the ratio of the real  $\sigma_{\text{bw}}^2$  to the high-bandwidth case,  $\sigma_{\text{bw,high}}^2$ . It is therefore the same quantity that is plotted on the right-hand side of Fig. 1. Equation (25) is used for the few cases in Section 4.1 for which the high-bandwidth approximation turns out not to be sufficiently accurate.

We conclude this section with a few physical interpretations of equations (21) and (23). We first point out that, because of the proportionality  $f_{\text{T}} \propto \lambda_c^{-1}$  in equation (14),  $t_{i,\text{max}}$  does not depend on the wavelength of observation. This independence originates from the fact that the quantity of concern is the angle of arrival of the wavefront, which is independent of the correction wavelength,  $\lambda_c$ . Nevertheless, and as expected, both error terms in equation (21)

depend on  $\lambda_c$  in such a way that a higher Strehl ratio is obtained at longer wavelengths.

We also note that the tilt measurement error,  $\sigma_{\text{ph}}^2$ , does not depend on  $D_r$ . While more photons are collected with a larger reception telescope, the precision needed in the differential tilt determination also increases with  $D_r$ . This result is in accordance with and explained by Foy et al. (1995). A slight dependence on  $D_r$ , favouring large telescopes, enters equation (21) through  $f_{\text{TZ}}$ .

At constant laser intensity in the mesosphere, the return flux,  $\Phi_p$ , is directly proportional to the area of the laser spot in the mesosphere, which is proportional to  $D_c^{-2}$ . Thus, equation (23) shows that, for a constant intensity,  $S_{\text{tilt}}$  does not depend on the size of the laser spot in the mesosphere. However, if the spot size is decreased at constant laser power, the intensity in the spot and with it the return flux per spot area (or the ‘brightness’ of the PLGS) increases. This increase in return flux is linear with intensity (or, in other words, proportional to  $D_c^2$ ) before saturation of the sodium transitions and approximately proportional to the square root of the laser intensity (proportional to  $D_c$ ) for intensities higher than saturation. Thus, the Strehl ratio of the tilt measurement will increase with decreasing laser spot size. As already mentioned in Section 2, it is therefore desirable to produce the smallest possible laser spot in the mesosphere, favouring a large emission telescope with an AO system.

In summary, we have shown that the performance of a tilt correction system with a PLGS improves with increasing diameter of both the emission and the reception telescopes and that an AO system for the emission telescope is desirable. (It is clear, that a compromise between increased performance on one hand and system cost and saturation effects on the other hand needs to be found.) It should be obvious that increasing the return flux from the PLGS, for example by increasing the laser power or duty cycle, and increasing the magnitude of the dispersion effect by using a larger difference between the wavelengths of the two lasers also improve the performance. These two effects are represented in equation (21) by the dependence of  $S_{\text{tilt}}$  on  $\Phi_p$  and  $\Delta n$ . Finally, and as always, the quality of the atmospheric conditions of the site, that is, the magnitude of the tilt coherence frequency,  $f_{\text{TZ}}$ , has a large influence on the Strehl ratio achieved by the system.

#### 4.1 Performance estimates of possible ELP-OA systems

In order to calculate the expected performance of the proposed ELP-OA system, we first need to obtain an estimate of the tilt coherence frequency  $f_{\text{TZ}}$ . Tyler (1994) uses the HV<sub>5/7</sub> Hufnagel–Valley turbulence profile corresponding to  $r_0 = 5$  cm (Hufnagel 1974), and a wind profile from Air Force Cambridge Research Laboratories (1965). For  $\lambda_c = 0.5$   $\mu\text{m}$ ,  $D_r = 3.5$  m,  $r_0 = 5$  cm and  $\theta = 0$ , he finds  $f_{\text{TG}} = 7.44$  Hz for the G-tilt, which translates to  $f_{\text{TZ}} = 8.27$  Hz for the Z-tilt under the same conditions. In our effort to keep the treatment in this paper analytical, we apply this  $f_{\text{TZ}}$  to a turbulence profile with a constant wind velocity profile (as we have done before) and scale  $f_{\text{TZ}}$  with  $D_r$  and  $r_0$  according to equation (16). Scaling  $f_{\text{TZ}}$  with the aperture diameter of the reception telescope is independent of the specific turbulence profile and introduces no error. The scaling with  $r_0$  depends on the particular wind and turbulence profile. However, because turbulence has been shown to consist frequently of only a few (or even just one) strong layers (see, e.g., Vernin & Muñoz-Tuñón 1994; Tallon et al. 1992), this assumption will not usually introduce significant errors into the calculation. As was the case before, if more accurate results are needed for detailed design studies, numerical integrations of the turbulence and wind profiles can be performed. Within the framework of this paper this is, how-

ever, not necessary, as we only attempt to outline the procedure and to obtain an impression of the general feasibility of the PLGS concept.

The conditions used by Tyler result in a wind speed  $V = vD_r = 9.3$  m s<sup>-1</sup> in equation (16). With  $D_r = 1.52$  m, we then obtain values for  $f_{\text{TZ}}$  of between 9.5 and 4.5 Hz for values of  $r_0$  ranging from 5 to 11 cm. It further needs to be noted that these values are the  $f_{\text{TZ}}$  values at  $\lambda_c = 0.5$   $\mu\text{m}$  and that  $f_{\text{TZ}}$  scales as  $\lambda_c^{-1}$ .  $f_{\text{TZ}}$  therefore also needs to be multiplied by  $(0.5 \mu\text{m})/\lambda_c$  in the following calculations.

While these values appear surprisingly low, they are in good agreement with both theoretical predictions and experimental results found by other authors, for example, Glindemann (1997) for the 3.5-m telescope at Calar Alto, Close & McCarthy (1994) for the 2.3-m telescope on Kitt Peak, or Dekens et al. (1994) and Chanan et al. (1996) for the Keck telescopes on Mauna Kea. Care must be taken, however, because the quoted frequencies do not always refer to exactly the same quantities. Different definitions of the tilt coherence frequencies appear in the literature and sometimes the quoted value refers to the ‘break frequency’, that is, the frequency at which the ‘kink’ in the tilt power spectrum occurs. While all of these values are of the same order of magnitude, they are not strictly comparable. Whenever we talk about the tilt coherence frequency in this paper, we refer to  $f_{\text{TZ}}$  in the sense of Tyler (1994) as defined in equations (14) and (16).

If light at 330 and 589.6 nm is used for the tilt measurement,  $(n - 1)/\Delta n = 25$  (Foy et al. 1995). The transmissivity of the atmosphere at 330 nm is approximately 0.3 at low altitudes (Allen 1976; Foy et al. 2000b). Following Foy et al. (1995), we use an instrument and detector efficiency of approximately 0.26 (two telescope mirrors at 0.85, transmission of instrument of 0.6, detector quantum efficiency 0.6) such that  $\eta \approx 0.08$ . Having specified the entire tilt correction system at this point, we now present different aspects of the system performance.

In Fig. 2, we show the Strehl ratio,  $S_{\text{tilt}}$ , calculated from equation (21) as a function of integration time for several astronomical observation bands and  $r_0 = 10$  cm (at 0.5  $\mu\text{m}$ ) for the configuration denoted ‘ELP-OA I’ in Table 1. It is clearly visible that the optimum integration time,  $t_{1,\text{max}}$ , is independent of wavelength as we have

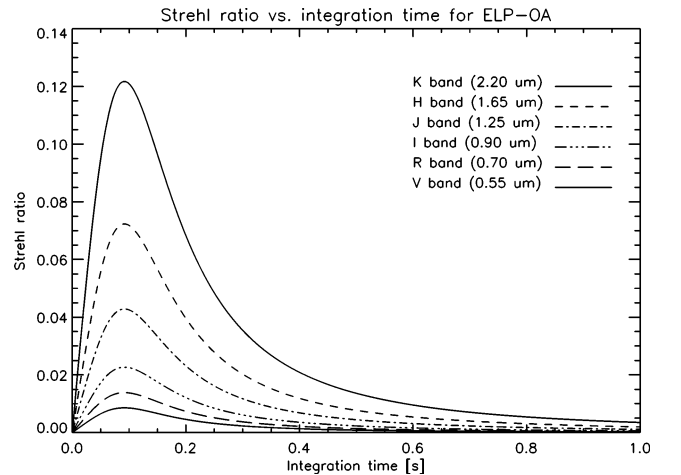


**Figure 2.** Strehl ratio versus integration time for several astronomical observation bands for the original configuration of ELP-OA (‘ELP-OA I’ in Table 1) and  $r_0 = 10$  cm (at 0.5  $\mu\text{m}$ ). The high-bandwidth approximation was used to calculate these results. The optimal integration time,  $t_{1,\text{max}}$ , is 92 ms.

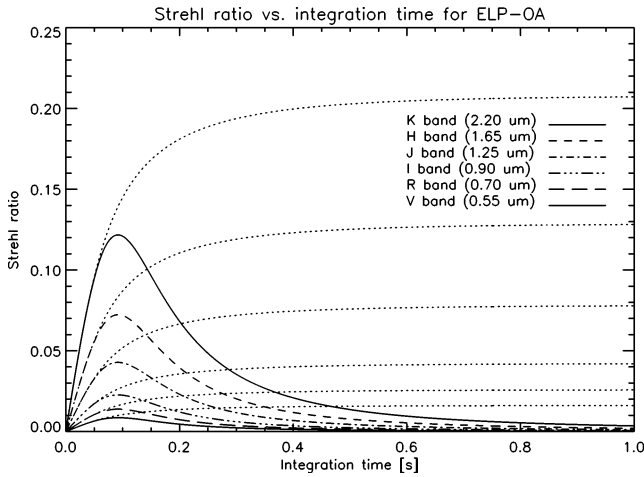


**Figure 3.** Plots of the same data as in Fig. 2. In addition, the Strehl ratios using the exact equations for the bandwidth error are plotted as dotted lines.

shown theoretically in Section 4. The maxima of all curves are at 92 ms as can be verified using equation (23).

One would therefore assume that the maximum attainable Strehl ratio of the ELP-OA I system is given by the 92-ms value of the curves. This is, however, not the case, as Fig. 2 has been calculated using the high-bandwidth approximation,  $f_c = (2\pi t_i)^{-1} \geq 4 f_{TZ}$  (Tyler 1994), which is clearly not the case for this example. We thus need to calculate the exact  $S_{\text{tilt}}$ , using equation (25) and the correction factor,  $c_i(t)$ . The results are shown in Fig. 3 as dotted lines. For ease of comparison, the results from Fig. 2 are repeated here. It seems at first peculiar that the exact curves do not display maxima but keep increasing with increasing integration time. This is, however, readily explained using Fig. 1.  $\sigma_{\text{bw}}^2$  does not increase indefinitely with  $t_i$ , but converges towards a constant value, which is simply the tilt variance of uncorrected turbulence. For the ELP-OA I case, the return flux from the PLGS is so low that the photon noise variance,  $\sigma_{\text{ph}}^2$ , dominates even for relatively long integration times and suppressed the occurrence of maxima in the curves in Fig. 3. The best Strehl ratio is obtained for very large values of  $t_i$ , when  $\sigma_{\text{ph}}^2$  approaches zero and  $\sigma_{\text{bw}}^2$  becomes constant. This is equivalent to not performing any tilt correction at all and the values towards which the dotted curves tend in Fig. 3 are in good agreement with the low-bandwidth limit given by Tyler (1994) for the Z-tilt (Tyler’s equation 90). The ELPOA I configuration is therefore not sufficient to produce a tilt correction in a long-exposure image. There exist, however, many possibilities to improve the performance of the system described above.

Improvements of the PLGS performance with respect to the ELPOA I case can be achieved with relatively simple means by using left-circularly polarized laser light [increase of the return flux by a factor between 1.2 and 1.5 (Jeys et al. 1992)] and by measuring the differential tilt between wavelengths of 330 nm and 2.3  $\mu\text{m}$  [decreasing  $(n-1)/\Delta n$  from 25 to 18]. The inclusion of infrared wavelengths also means that the measurement error produced by the infrared light in equation (7) is negligible with respect to the 330-nm light (Foy et al. 1995).  $\sigma_{\text{ph}}^2$  is therefore reduced by a factor of 2 in equations (10)–(25). Laser technology has progressed to the point where a laser with  $P = 25$  W,  $f_{\text{rep}} = 30$  kHz and  $\tau_p = 70$ –80 ns seems feasible for use in Phase 2 of ELP-OA. With this new configuration, denoted ‘ELP-OA II’ in Table 1, the PLGS system can achieve the Strehl ratios shown in Fig. 4. We can now see that a maximum shows up in the

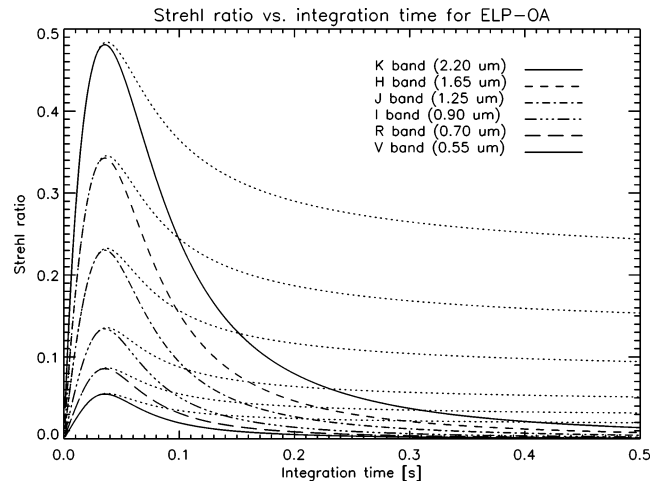


**Figure 4.** Strehl ratio versus integration time for several astronomical observation bands for the configuration denoted ‘ELP-OA II’ in Table 1 and  $r_0 = 10$  cm. Solid and dashed lines, high-bandwidth approximation; dotted lines, exact solution. The optimal integration time,  $t_{i,\text{max}}$ , is 35 ms.

exact curves (dotted lines) for  $S_{\text{tilt}}$ . This maximum is approximately twice as high as the uncorrected tilt Strehl ratio (the asymptotic limit for large integration times) for all wavelength bands shown. An experimental verification of this effect should be possible, in particular at infrared wavelengths. We also note that the approximations (solid and dashed lines) produce almost the same results for both the location (35 ms) and the magnitudes of the maxima as the exact curves (dotted lines). Since all the following examples work in a regime where the approximation is even more accurate than in Fig. 4, it suffices to work with the high-bandwidth approximation from here on.

As we mentioned in Section 3, we expect another significant improvement of system performance from implementing a ‘modeless laser’, which could produce an increase of return flux of up to a factor of 10. If this increase turns out to be realistic, we arrive at the Strehl ratios shown in Fig. 5 as a function of wavelength. In this and all the following figures, only the maximum Strehl ratios, that is, the Strehl ratios obtained for the optimum integration times are

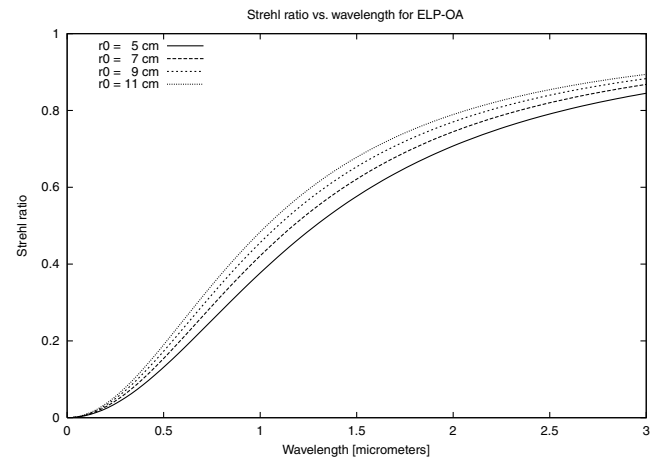


**Figure 5.** Maximum Strehl ratio versus wavelength for values of  $r_0$  ranging from 5 to 11 cm for the original configuration denoted ‘ELP-OA III’ in Table 1. Optimal integration times range from 12 ms ( $r_0 = 5$  cm) to 19 ms ( $r_0 = 11$  cm).

plotted. The parameters used to produce Fig. 5 are summarized under ‘ELP-OA III’ in Table 1. Optimal integration times range from 12 ms ( $r_0 = 5$  cm) to 19 ms ( $r_0 = 11$  cm) for this setup. In the near-infrared, very high Strehl ratios are obtained and the implementation of a PLGS at an AO system would not degrade the performance significantly with respect to using a natural tilt guide star while yielding 100 per cent sky coverage. An equally high Strehl ratio cannot be obtained at visible wavelengths for ELP-OA. However, the goal of the ELP-OA project has never been to build a PLGS adaptive optics system at a small (1.5-m) telescope at a low-altitude site. Its goal is to serve as a test bed for the implementation of such a system at a large (8-m or greater diameter) telescope at a good astronomical site. This demonstration should be possible at both infrared and visible wavelengths.

Summarizing this section, we believe that we have collected sufficient evidence to show that the feasibility of the PLGS concept can be verified experimentally in the second phase of ELP-OA. The results of these experiments will serve as tests if any of the assumptions made in this section need to be adjusted. However, even if this turns out to be the case, we are confident that ongoing development in particular of CuHBr lasers should soon allow a PLGS tilt system to produce high Strehl ratios at least at near-infrared wavelengths at a telescope such as the OHP 1.52-m telescope. Apart from an increase of pulse repetition rate and pulse length for pulse lasers, the most promising developments could be the arrival of modelless lasers and of continuous wave (CW) lasers with output powers of tens of watts.<sup>2</sup> The use of these kinds of lasers would eliminate the saturation of mesospheric sodium (see Table 2) and increase the photon return flux for a fixed average laser power significantly with respect to pulsed lasers.

## 5 IMPLEMENTATION AT A LARGE ASTRONOMICAL TELESCOPE

Implementing a PLGS tilt correction system at a large telescope at a good astronomical site will produce higher Strehl ratios than those found for the systems investigated in the previous section. This is mostly caused by the better atmospheric conditions, translating into a smaller  $f_T$  in equation (21) and fewer losses owing to atmospheric absorption and scattering. A second, albeit much smaller gain, is caused by the larger radius of the reception telescope,  $D_r$  (see equation 14).

As an example of a PLGS system at a site such as Cerro Paranal or Mauna Kea, we use the system parameters of the fourth column, denoted ‘8-m I’, in Table 1. For the tilt coherence time, we use the same single-layer model as before ( $V = 9.3$  m s<sup>-1</sup>), but now with  $D_r = 8$  m and  $r_0$  ranging from 15 to 25 cm. We then obtain values of  $f_{TZ}$  between 2.9 and 1.9 Hz. The atmospheric transmission at 330 nm at a high-altitude site is approximately 0.5 leading to  $\eta \approx 0.13$ . Because of the better seeing, we can also afford to use a larger emission telescope ( $D_e = 0.5$  m) without introducing any additional complexity compared with the ELP-OA system.

Using the system parameters of Table 1 and equation (2), we find  $I_c = 6.8 \times 10^5$  W m<sup>-2</sup>, which is approximately 1.5 times higher than the intensity for the ELP-OA I configuration. In order to obtain an estimate of the expected return flux, we assume that  $\Phi_p$  increases approximately as  $\sqrt{I_c}$  in the saturated regime if everything else

<sup>2</sup>Of course, it is also likely that pulse lasers with much higher output power will become available. It is, however, debatable whether one would wish to install such a high-power laser at an astronomical site.

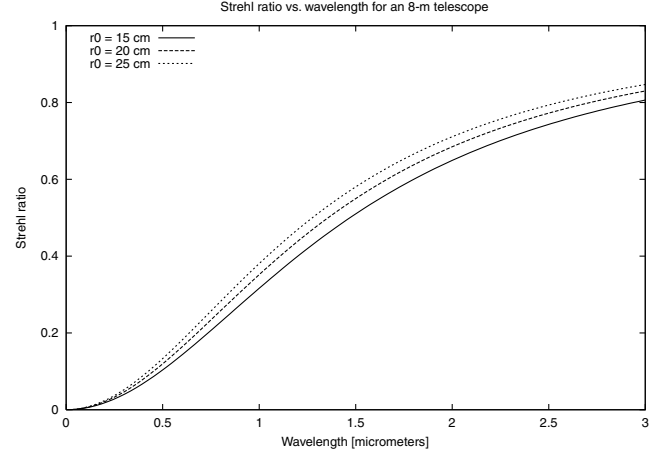


**Figure 6.** Maximum Strehl ratio versus wavelength for values of  $r_0$  ranging from 15 to 25 cm for the 8-m configuration denoted ‘8-m I’ in Table 1. Optimal integration times range from 42 ms ( $r_0 = 15$  cm) to 56 ms ( $r_0 = 25$  cm).

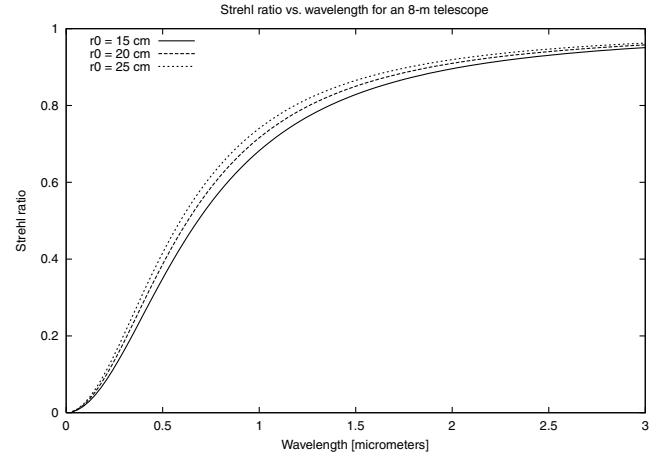


**Figure 7.** Maximum Strehl ratio versus wavelength for values of  $r_0$  ranging from 15 to 25 cm for the 8-m configuration denoted ‘8-m II’ in Table 1. Optimal integration times range from 20 ms ( $r_0 = 15$  cm) to 26 ms ( $r_0 = 25$  cm).

remain unchanged. After taking all relevant parameters into account we thus expect  $\Phi_p \approx 7.0 \times 10^4$  photon s<sup>-1</sup> m<sup>-2</sup>.

Combining all of these values and using a pulse laser system with left-circularly polarized light (the complete list of parameters is given under ‘8-m I’ in Table 1), we obtain the results shown in Fig. 6. Optimal integration times are found to range from 42 ms ( $r_0 = 15$  cm) to 56 ms ( $r_0 = 25$  cm). We see that we can achieve a good correction at infrared wavelengths but that the correction at visible wavelengths is not acceptable for use with an AO system. If we further apply the expected increase in return flux owing to a modelless laser to an otherwise identical system (the parameters are listed under ‘8-m II’ in Table 1), we find high Strehl ratios even at visible wavelengths (Fig. 7). Optimal integration times are found to range from 20 ms ( $r_0 = 15$  cm) to 26 ms ( $r_0 = 25$  cm) for this configuration.

We have mentioned before that using different laser configurations (different pulse lengths or repetition rates, pulsed versus continuous wave lasers, etc.) produces different results for an otherwise identical setup. We might therefore want to ask a different question than before by requiring a certain Strehl ratio at a given wavelength

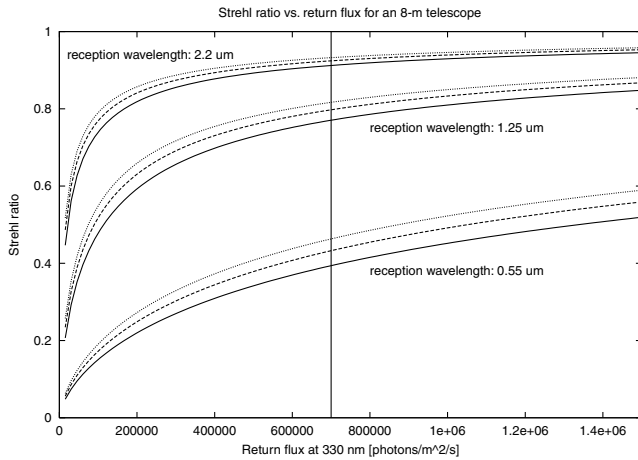


**Figure 8.** Maximum Strehl ratio versus return flux at 330 nm for the 8-m configurations of Table 1. The set of three curves with the highest values is calculated for tilt correction in the *K* band (2.20  $\mu\text{m}$ ), the middle set is for the *J* band (1.25  $\mu\text{m}$ ), and the bottom set is for the *V* band (0.55  $\mu\text{m}$ ). The three curves in each set correspond to different values of  $r_0$ : 15 cm (solid lines), 20 cm (dashed lines) and 25 cm (dotted lines). The return flux used is the flux before accounting for atmospheric and instrument transmission and thus corresponds to the variable  $\Phi_P$  as it is used throughout this paper. The vertical line indicates the setup used in Fig. 7, that is,  $\Phi_P \approx 7.0 \times 10^5$  photon  $\text{s}^{-1} \text{m}^{-2}$ .

and trying to find the laser configuration that best matches these requirements. This kind of problem can also be investigated using the formalism of this paper as we demonstrate in Fig. 8. Therein we show  $S_{\text{ilt}}$  as a function of the return flux from the PLGS at 330 nm,  $\Phi_P$ , for three different wavelengths and three values of  $r_0$ . The system setup used is equivalent to that of Fig. 7 with the exception that we make no assumptions concerning the lasers. (As an orientation, the laser configuration and respective return flux used in Fig. 7 is indicated by the vertical line.) Any laser producing a given return flux can be used to achieve the respective Strehl ratio.

As a final example, we demonstrate the effect of changing atmospheric conditions on the performance of the PLGS system. Up to this point we have always assumed that we have perfect knowledge of  $r_0$  (or the turbulence profile if we cannot assume a constant wind velocity profile) and thus of the tilt coherence time,  $f_{\text{TZ}}$ , and that we can therefore apply the optimum integration time at any instant. In reality, we might want to measure  $r_0$  only sporadically, or even simply use an average value for the site, and work with a fixed  $t_i$  in between measurements. It is important to understand the implications of such an approach for the performance of the PLGS system.

In Fig. 9 we show the effect of a changing  $r_0$  on the performance of the system. Three sets of curves are shown for observations in the astronomical *K* (2.20  $\mu\text{m}$ ), *J* (1.25  $\mu\text{m}$ ) and *V* (0.55  $\mu\text{m}$ ) bands for the same system that was used for Fig. 7. Each curve is a plot of the Strehl ratio versus the atmospheric coherence length,  $r_0$ , for the same constant velocity profile with  $V = 9.3 \text{ m s}^{-1}$  that was used before. The solid lines are calculated using the best integration time,  $t_{i,\text{max}}$ , for the given conditions ( $r_0$ ,  $f_{\text{TZ}}$ ). The crosses and diamonds show the performance of the system if the  $t_{i,\text{max}}$  optimized for  $r_0 = 15 \text{ cm}$  (diamonds) and  $30 \text{ cm}$  (crosses) are used instead. We can see that the degradation in Strehl ratio is insignificant over a wide range of  $r_0$  if the Strehl ratio is high in the first place. For lower Strehl ratios, however, one might find a significant decrease in performance if

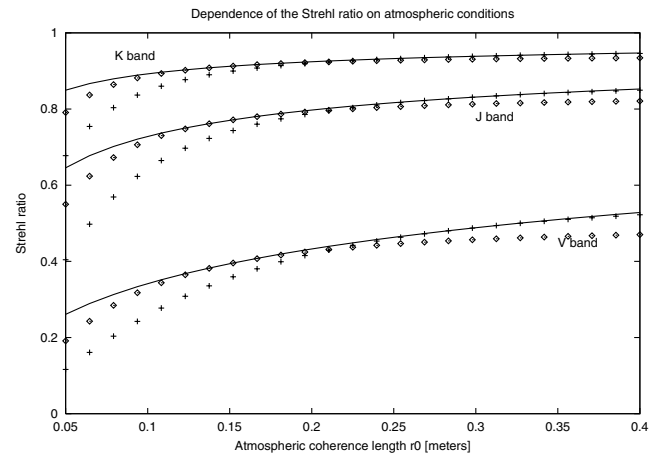


**Figure 9.** Maximum Strehl ratio versus  $r_0$  at 0.5  $\mu\text{m}$  for the same system that was used in Fig. 7. Three sets of curves are shown for observations in the astronomical *K* (2.20  $\mu\text{m}$ ), *J* (1.25  $\mu\text{m}$ ) and *V* (0.55  $\mu\text{m}$ ) bands. The solid lines show the Strehl ratio if the best integration time,  $t_{i,\text{max}}$ , for the given conditions ( $r_0$ ,  $f_{\text{TZ}}$ ) is used. The crosses and diamonds show the performance of the system if the  $t_{i,\text{max}}$  optimized for  $r_0 = 15 \text{ cm}$  (diamonds) and  $30 \text{ cm}$  (crosses) are used.

one does not work with an optimized integration time. The need for frequent – or continuous – measurements of the turbulence profile will therefore depend on the particular site, PLGS system and Strehl ratio requirements. The formalism of this paper in combination with data from site testing campaigns can be used to investigate whether such an approach is necessary for a given system.

## 6 CONCLUSIONS

We have developed a formalism that permits us to analyse the performance of adaptive optics systems that use polychromatic laser guide stars for tilt sensing. This formalism was originally developed as a design study for ELP-OA, a project in which we intend to demonstrate the feasibility of the PLGS concept experimentally. It can also be used to predict the performance of an astronomical adaptive optics system that uses a PLGS as its tilt guide star. Such a system would be completely independent of natural guide stars and obtain 100 per cent sky coverage.

We have demonstrated that ELP-OA is feasible and that a verification of the PLGS concept should be possible at visible and near-infrared wavelengths using existing laser technology. It has also become clear that the original design of ELP-OA is not sufficient for this purpose. We suggest modifications to this design and show that the system performance can be improved significantly with respect to the original design. We expect the tilt correction system to produce high Strehl ratios at near-infrared wavelengths if a system similar to the ELP-OA system is moved to a high-altitude astronomical site. Medium Strehl ratios can be attained at visible wavelengths. We show how to use the formalism of this paper to determine the laser requirements to satisfy performance specifications of a PLGS system. We also demonstrate the effect of changing conditions of atmospheric turbulence on the performance of the system.

## REFERENCES

Air Force Cambridge Research Laboratories, 1965, Handbook of Geophysics and Space Environments. McGraw-Hill, New York

Allen C.W., 1976, *Astrophysical Quantities*. The Athlone Press, Univ. London

Avicola K. et al., 1994, *J. Opt. Soc. Am. A*, 11, 825

Beckers J.M., 1988, in Ulrich M.-H., ed., *Very Large Telescopes and their instrumentation*, ESO Conf. no. 30. ESO, Garching, Germany, p. 693

Belenkii M.S., 2000, *Appl. Opt.*, 39, 6097

Belenkii M., Karis S.J., Brown J.M., II, Fugate R.Q., 1999, *Opt. Lett.*, 24, 637

Bellanger V., 2002, PhD thesis, Université Paris VI, Paris, France

Biegert J., Diels J.-C., Milonni P.W., 2000, *Opt. Lett.*, 25, 683

Bonaccini D., Prieto E., Corporon P., Le Mignan D., Prado P., Gredel R., Hubin N., Christou J., 1997, in Proc. SPIE, Vol. 3136, Performance of the ESO AO system, Adonis, at La Silla 3.6 m telescope. SPIE, Bellingham, p. 589

Chanan G., Djorgovski G., Gleckler A., Kulkarni S., Mast T., Max C., Nelson J., Wizinowich P., 1996, *Adaptive optics for Keck Observatory*, Technical report, California Institution for Research in Astronomy, 5-4

Close L.M., McCarthy D.W., 1994, *Pub. Astron. Soc. Pacific*, 106, 77

Coutance P., Pique J.-P., 1998, *IEEE J. Quantum Electron.*, 34, 1340

Coutance P., Naylor G., Pique J.-P., 1995, *IEEE J. Quantum Electron.*, 31, 1747

Davies R., Hippler S., Hackenberg W., Ott T., Butler D., Kasper M., Quirrenbach A., 2000, *Exper. Astron.*, 10, 103

Dekens F., Kirkman D., Chanan G.A., Mast T.S., Nelson J.E., Illingworth G., Wizinowich P.L., 1994, in Mark A. Ealey., Fritz Merkle, eds, Proc. SPIE Vol. 2201, *Adaptive Optics in Astronomy*. SPIE, Bellingham, pp. 310–313

Ellerbroek B.L., 1994, *J. Opt. Soc. Am. A*, 11, 783

Esposito S., Ragazzoni R., Riccardi A., O’Sullivan C., Ageorges N., Redfern M., Davies R., 2000, *Exper. Astron.*, 10, 135

Ewart P., 1985, *Opt. Commun.*, 55, 124

Foy R., Labeyrie A., 1985, *A&A*, 152, L29

Foy R., Migus A., Biraben F., Grynberg G., McCullough P.R., Tallon M., 1995, *A&A Supl*, 111, 569

Foy R. et al., 2000a, in Proc. SPIE, Vol. 4007, *Adaptive Optical Systems Technology*. SPIE, Bellingham

Foy R. et al., 2000b, *J. Opt. Soc. Am. A*, 17, 2236

Froc G., Rosencher E., Atal-Trétout B., Michau V., 2000, *Opt. Commun.*, 178, 405

Fugate R.Q. et al., 1994, *J. Opt. Soc. Am. A*, 11, 310

Glindemann A., 1997, *Pub. Astron. Soc. Pac.*, 109, 682

Glindemann A., Hippler S., Berkefeld T., Hackenberg W., 2000, *Exper. Astron.*, 10, 5

Hufnagel R.E., 1974, in *Digest of Topical Meeting on Optical Propagation through Turbulence*. OSA, Washington, DC, p. WA1

Jeys T.H., Heinrichs R.M., Wall K.F., Korn J., Hotaling T.C., Kibblewhite E., 1992, *Opt. Lett.*, 17, 1143

Le Louarn M., Foy R., Hubin N., Tallon M., 1998, *MNRAS*, 295, 756

Milonni P.W., Fugate R.Q., Telle J.M., 1998, *J. Opt. Soc. Am. A*, 15, 217

Morris J., 1994, *J. Opt. Soc. Am. A*, 11, 832

Olivier S.S. et al., 1999, in Tyson R.K., Fugate R.Q., eds, Proc. SPIE, Vol. 3762, *Adaptive optics systems and technology*. SPIE, Bellingham

Parenti R.R., Sasiela R.J., 1994, *J. Opt. Soc. Am. A*, 11, 288

Pilkington J., 1987, *Nat*, 330, 116

Rigaut F. et al., 1998, *Pub. Astron. Soc. Pac.*, 110, 152

Roddier F., 1993, in Robertson J.G., Tango W.J., eds, Proc. IAU Symp., *High Angular Resolution Imaging*. Kluwer, Dordrecht

Sandler D.G., Stahl S., Angel J., Lloyd-Hart M., McCarthy D., 1994, *J. Opt. Soc. Am. A*, 11, 925

Schöck M., Foy R., Pique J.P., Tallon M., Segonds P., Laubscher M., Peillet O., 1999, in Tyson R.K., Fugate R.Q., eds, Proc. SPIE, Vol. 3762, *Adaptive Optics Systems and Technology*. SPIE, Bellingham, p. 321

Séchaud M., Hubin N., Brixon L., Jalin R., Foy R., Tallon M., 1988, in Ulrich M.-H., ed., *Very Large Telescopes and their Instrumentation*, ESO/NOAO Conf. no 30. ESO, Garching, Germany, p. 705

Tallon M., Foy R., 1990, *A&A*, 235, 549

Tallon M., Foy R., Vernin J., 1992, in Ulrich M.-H., ed., *Progress in telescope and instrumentation technologies*, ESO Conf. no 42. ESO, Garching, Germany, p. 517

Tokovinin A., 2000, *MNRAS*, 316, 637

Troy M. et al., 2000, in Peter L. Wizinowich, ed., Proc. SPIE Vol. 4007, *Adaptive Optical Systems Technology*. SPIE, Bellingham, pp. 31–40

Tyler G.A., 1994, *J. Opt. Soc. Am. A*, 11, 358

Vaillant J., Thiébaud É., Tallon M., 2000, in Wizinowich P.L., ed., Proc. SPIE, Vol. 4007, *Adaptive Optical Systems Technology*. SPIE, Bellingham, p. 308

Vernin J., Blazit A., Mourard D., 2000, in Wizinowich P. L., ed., Proc. SPIE Vol. 4007, *Adaptive Optical Systems Technology*. SPIE, Bellingham, pp. 999–1010

Vernin J., Muñoz-Tuñón C., 1994, *A&A*, 284, 311

Wizinowich P. et al., 2000, *Pub. Astron. Soc. Pac.*, 112, 315

## APPENDIX A: HALO CONTRIBUTION TO THE ERROR BUDGET

In this appendix we derive the tilt correction error if the seeing-limited halo of the PLGS is taken into account. The derivation is analogous to the derivation of the photon noise in Section 4. The only difference is that the spot size of the halo and the number of photons returned from the halo have to be considered in equations (4) and (7) in addition to the spot size of and return flux from the core. The photon noise term is now a weighted average of the contributions from the core and the halo. If we assume again that a fraction  $S_e$  of the return flux comes from the core and the rest,  $1 - S_e$ , comes from the halo, we can write  $\sigma_{\text{ph}}^2$  as

$$\sigma_{\text{ph}}^2 = \left( \frac{n-1}{\Delta n} \right)^2 \frac{16}{\pi^3} \frac{\lambda_e^2}{\eta \Phi_P D_r^2 t_i} \left[ \frac{S_e}{D_e^2} + \frac{1-S_e}{r_0^2} \right]. \quad (\text{A1})$$

This changes only the definition of the constant  $a$  in equation (22) and therefore the explicit form of the optimum integration time,  $t_i$  in equation (23), while the general form of  $t_i$  remains unchanged. We thus obtain

$$t_i = \left( \frac{a}{2b} \right)^{1/3} = 0.187 \left[ \left( \frac{n-1}{\Delta n} \right)^2 \frac{\lambda_e^2}{\eta \Phi_P \lambda_c^2 f_T^2} \left( \frac{S_e}{D_e^2} + \frac{1-S_e}{r_0^2} \right) \right]^{1/3}. \quad (\text{A2})$$

We see that equations (A1) and (A2) reduce to equations (10) and (23) when the Strehl ratio of the emission system approaches unity.

This paper has been typeset from a  $\text{\TeX}/\text{\LaTeX}$  file prepared by the author.